ELSEVIER

Tectonophysics 312 (1999) 133–155

TECTONOPHYSICS

www.elsevier.com/locate/tecto

Development of preferred orientation and microstructure in sheared quartzite: comparison of natural data and simulated results

Toru Takeshita [a,*], Hans-Rudolf Wenk [b], Ricardo Lebensohn [c]

[a] *Department of Earth and Planetary Systems Science, Hiroshima University, Higashi-Hiroshima 739-8526, Japan*
[b] *Department of Geology and Geophysics, University of California, Berkeley, CA 94720, USA*
[c] *Instituto de Fisica Rosario (UNR–CONICET), 27 de Febrero 210 Bis, 2000 Rosario, Argentina*

Received 26 May 1998; accepted 21 May 1999

Abstract

c-axis fabric and microstructures in a quartzite sample, sheared and extensively recrystallized under greenschist facies conditions, have been analyzed and compared with theoretical predictions using a viscoplastic self-consistent model modified to incorporate the effects of dynamic recrystallization. An asymmetric small-circle *c*-axis fabric about the finite shortening *z*-axis with a small half opening angle (35°) is present in the sample; it consists of four orientation components which are represented by host grain *c*-axis orientations (referred to as A, B, C and D): A and B are at high angles to the foliation plane, displaced against and with the sense of shear, respectively; C is in an intermediate direction between the *Y*- and *Z*-axis of finite strain, and D forms a subsidiary concentration around the intermediate strain (*Y*-) axis. B- and C-grains are favorably oriented for basal (0001) and pyramid $\{10\bar{1}1\}\langle a\rangle$ slip, respectively, and strongly deformed, while A- and D-grains are unfavorably oriented for the slip systems and little or moderately deformed. Some of A-grains are even fractured. The degree of dynamic recrystallization increases with increasing strain undergone by differently oriented grains (in the sequence of A-, D-, C- and B-grains). Microstructural evidence and theoretical predictions indicate that harder A-, C- and D-grains were significantly consumed by the grain boundary migration of the softer recrystallized B-component (although the consumption of A-grains was not really documented in the quartzite sample). The conclusion is supported by the fact that the B-component is much more dominant in the recrystallized than in the host *c*-axis fabric. Hence, the *c*-axis maximum nearly perpendicular to the shear plane and apparently displaced with the sense of shear commonly found in naturally sheared quartzites (correlated with the B-component) is presumably developed by the growth of soft orientations for basal (0001) slip by grain boundary migration at large strains.

Keywords: deformed quartzite; lattice preferred orientation; grain boundary migration; recrystallization

1. Introduction

The role of dynamic recrystallization in the development of lattice preferred orientation (referred to as LPO in this study) in deformed and recrystallized quartzite has remained enigmatic (e.g. Hobbs, 1968; Jessell, 1988a,b), and a better understanding of dynamic recrystallization in quartz is necessary if LPO patterns in recrystallized quartzite are used to interpret geological processes. Hirth and Tullis (1992) and Gleason et al. (1993) demonstrated that three

* Corresponding author. Tel.: +81 824 24 7474; Fax: +81 824 24 0735; E-mail: toru@letitbe.geol.sci.hiroshima-u.ac.jp

0040-1951/99/$ – see front matter
PII: S0040-1951(99)00173-0

different regimes of dynamic recrystallization can be identified in experimentally deformed quartzites: strain-induced grain boundary migration (GBM) at low T, subgrain rotation at medium T and GBM driven by grain boundary energy at high T. The kinematically induced LPO in quartz polycrystals resulting from intracrystalline slip is not greatly modified by rotation recrystallization, because the lattice orientations of the rotated subgrains are controlled by those of the host grains (e.g. Lloyd and Freeman, 1991, 1994; Gleason et al., 1993). Subgrain rotation recrystallization is important at relatively low strains. At larger strains migration recrystallization becomes dominant over subgrain rotation and this can greatly modify the LPOs (e.g. for olivine, Zhang and Karato, 1995; for norcamphor (quartz analogue), Herwegh and Handy, 1996), although the facts have not yet been demonstrated for quartz.

One driving force for grain boundary migration is the difference in the strain energy associated with dislocations between adjacent grains (e.g. Gottstein and Mecking, 1985; Humphreys and Hatherly, 1995). Since the deformation of individual grains is orientation-dependent, the strain energy is also. Therefore polycrystal plasticity models which predict strain energy in differently oriented grains can be used to predict processes during dynamic recrystallization. Wenk et al. (1997) have used a viscoplastic self-consistent model to simulate the LPO development caused by concurrent intracrystalline slip and grain boundary migration (i.e. nucleation and growth) in quartz and other materials. For quartz the results are promising because some of the LPO components, particularly the commonly observed and enigmatic *c*-axis maximum at *Y* (intermediate axis of finite strain) (e.g. Bouchez, 1977; Helming et al., 1994) can be explained.

For simple shear, polycrystal plasticity theories predict a *c*-axis fabric with internal asymmetry (Lister and Williams, 1979; Wenk et al., 1989). Referring to the internal asymmetry of *c*-axis fabric, the determination of sense of shear is unequivocal in naturally deformed quartzite (e.g. Law, 1990). Nevertheless, the *c*-axis fabric patterns are often significantly different between models and natural data. While asymmetric crossed girdles rotated against the sense of shear (relative to coaxial pure shear deformation) are predicted for model simple shear *c*-axis fabrics, single girdle or a maximum *c*-axis fabric rotated with the sense of shear is often developed in naturally sheared quartzite. The models are for deformation by slip, whereas the natural quartzites are generally recrystallized. In fact the shear experiments of Dell' Angelo and Tullis (1989) illustrate a *c*-axis maximum displaced against the sense of shear for low strain and a maximum displaced with the sense of shear for high strain where recrystallization occurs.

In this paper we make an attempt to reconcile the controversy about the effect of dynamic recrystallization on LPO development through a detailed analysis of microstructure and LPO in a quartzite sheared under greenschist facies conditions. By dividing the *c*-axis fabric into a few orientation components and relating crystal orientation and microstructure, it can be shown that grains belonging to each orientation group exhibit characteristic deformation and recrystallization features. The orientation-dependent deformation and recrystallization mechanisms in this natural quartzite are then discussed by comparing the microstructures with predictions from a deformation-based model of dynamic recrystallization.

2. Geological setting and sample description

The quartzite used in this study was selected among many metamorphic quartzites because of the wide variety of microstructural features associated with elements of preferred orientation. The sample Sci 490 is a quartz layer in a metasedimentary sequence from Val Albigna in the Bergell Alps of southeastern Switzerland. The metasediments compose the northern envelope of the Tertiary Bergell granite and were deformed and recrystallized concurrently with the emplacement of the granite (Wenk, 1973). Mylonitic textures, particularly of quartz, and regular foliations and lineations are widely present in the granite and adjacent rocks. The quartz layer perhaps originated from quartzite (quartz arenite), which alternates with metamorphosed pelitic layers consisting of muscovite, biotite, fibrolite, andalusite, garnet, plagioclase and quartz. The metamorphic mineral assemblages indicate temperature–pressure conditions of amphibolite facies ($>500^{o}$C).

3. Deformation and recrystallization microstructures

Both the *XZ* and *YZ* sections are prepared from the sample, where the *X*-, *Y*- and *Z*-axis denote elongation (lineation), intermediate and shortening (normal to the foliation) axes of finite strain, respectively (Fig. 1a). In this study, *c*-axis orientations of individual grains were measured with a U-stage for LPO analysis. Analyses of deformation and recrystallization microstructures such as equivalent diameter (described below) and aspect ratio of relict host grains, have been carried out with a petrographic microscope both in the *XZ* and *YZ* sections of the quartzite sample.

3.1. Microstructures indicative of shear strain

In the *XZ* section of sample Sci 490, a shear deformation with a top-to-the-northwest sense (i.e. thrust sense of shear) is indicated by C′-type shear bands (Berthé et al., 1979, or extensional crenulation

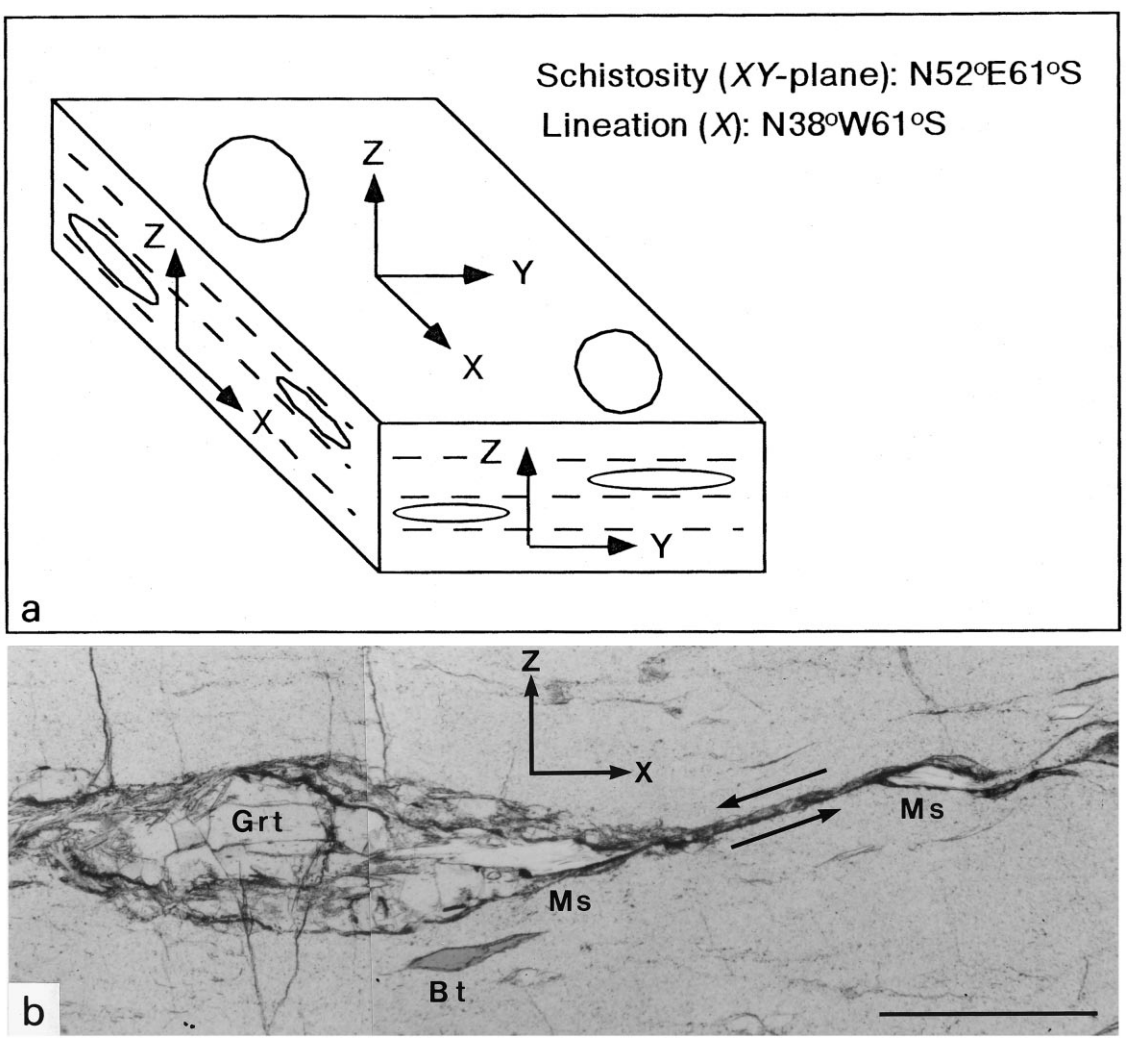

Fig. 1. (a) Schematic sketch of the quartzite sample and sample coordinates used for the microfabric analysis. (b) A shear band (micrographs, plane polarizers) indicative of shear strain in the *XZ* section of sample Sci 490 (the orientations of the *X*- and *Z*-axis are shown in the micrograph by arrows). A top-to-the-northwest sense of shear (shown by arrows) is inferred from the displacement of separated muscovite crystals. *Grt*, *Bt* and *Ms* denote garnet, biotite and muscovite, respectively. Scale bar 0.5 mm.

cleavage after Platt and Vissers, 1980) (Fig. 1b). The average trace of shear bands is rotated counterclockwise by 20º from the foliation plane about the *Y*-axis (SB in Fig. 2a). The top-to-the-northwest sense of shear conforms with the shear sense inferred from both the asymmetry of the quartz *c*-axis fabric and oblique foliation in recrystallized grains which are described below. It has been demonstrated that shear bands develop at a relatively small amount of shear strains ($\gamma > 2$) in experimentally sheared quartzites (Dell' Angelo and Tullis, 1989).

3.2. c-axis fabric components in host grains and inferred slip systems

Although recrystallization is extensive in quartz grains from the sample, the core of host grains is often preserved. Therefore, the *c*-axis fabric was analyzed separately for relict host and recrystallized grains. The *c*-axis fabric in relict host grains is very strong with a few well-defined components, named A, B, C and D (Fig. 2a,b). Here each *c*-axis orientation represents an average *c*-axis orientation in kinked or polygonized host grains (2–10 measurements have been performed in misoriented domains of each host grain). The host *c*-axis fabric consists of asymmetric small circle girdles about the *Z*-axis, rotated by 10º with the sense of shear about the *Y*-axis. The half opening angle of the small circles is approximately 35º. A small *c*-axis concentration exists close to the *Y*-direction, which could indicate that the small circle girdles are transitional to type I crossed girdles after Lister (1977). The small circle *c*-axis fabric with a small half opening angle suggests that the deformation took place under greenschist facies conditions (ca. 300–400ºC) (e.g. Lister and Dornsiepen, 1982; Takeshita and Wenk, 1988; Takeshita, 1996), correlative with regime II in experimentally deformed quartz aggregates by Hirth and Tullis (1992). It indicates that the deformation of quartz occurred during a retrograde stage after the peak metamorphism in amphibolite facies conditions evidenced by the metamorphic mineral assemblages.

The LPO of this sample has been previously investigated by neutron diffraction (Fig. 2c, Helming et al., 1994). From a deconvolution of the orientation distribution into components, the bulk texture can be described by a fairly large number of geometric components. Most of them are related pairwise by a 60º rotation about the *c*-axis indicating that the texture of this sample displays basically hexagonal crystal symmetry. The (0001) pole figure determined by neutron diffraction is similar to the host *c*-axis fabric measured with a U-stage (and more so to the composite *c*-axis fabric shown in Fig. 8a). It should be emphasized that in this paper we only discuss the *c*-axis fabric, rather than the full crystal orientation, and conclusions are therefore limited.

The quartz *c*-axis fabric pattern has a triclinic symmetry with some approximation to monoclinic symmetry. This low symmetry suggests that the deformation was non-coaxial. In the *c*-axis fabric, an incomplete crossed girdle containing the *Y*-axis rotated *with* the sense of shear, and one rotated *against* it which merges the former girdle at intermediate directions between the *Z*- and *Y*-axis could be distinguished (Fig. 2). These two incomplete girdles of the *c*-axis fabric can be correlated with the leading and trailing edges of the asymmetrical crossed girdle *c*-axis fabric described by Law (1987), caused by a simple-shear dominated deformation, with the top to the northwest.

Orientation components A, B, C and D, distinguished in the host *c*-axis fabric (Fig. 2b) show characteristic deformation and recrystallization microstructures. A is a maximum at high angles to the foliation plane, displaced against the sense of shear, and B is a similar maximum displaced with the sense of shear. C represents asymmetrical concentrations in intermediate directions between the *Z*- and *Y*-axis, and D is a subsidiary concentration around the *Y*-axis.

3.2.1. Component A ('A-grains').

Most of A-grains appear as relatively undeformed globular grains, although they are commonly polygonized (or kinked) (Fig. 3), suggesting that these are relict grains surviving dynamic recrystallization. It is thus concluded that A-grains were not favorably oriented during most of the non-coaxial strain history for the activation of basal (0001) slip which was dominant as inferred below. Similar moderately deformed globular grains have been reported in many of natural quartzites deformed in coaxial strain paths with *c*-axes parallel to the *Z*-axis (e.g. Bouchez, 1977; Law et al., 1984).

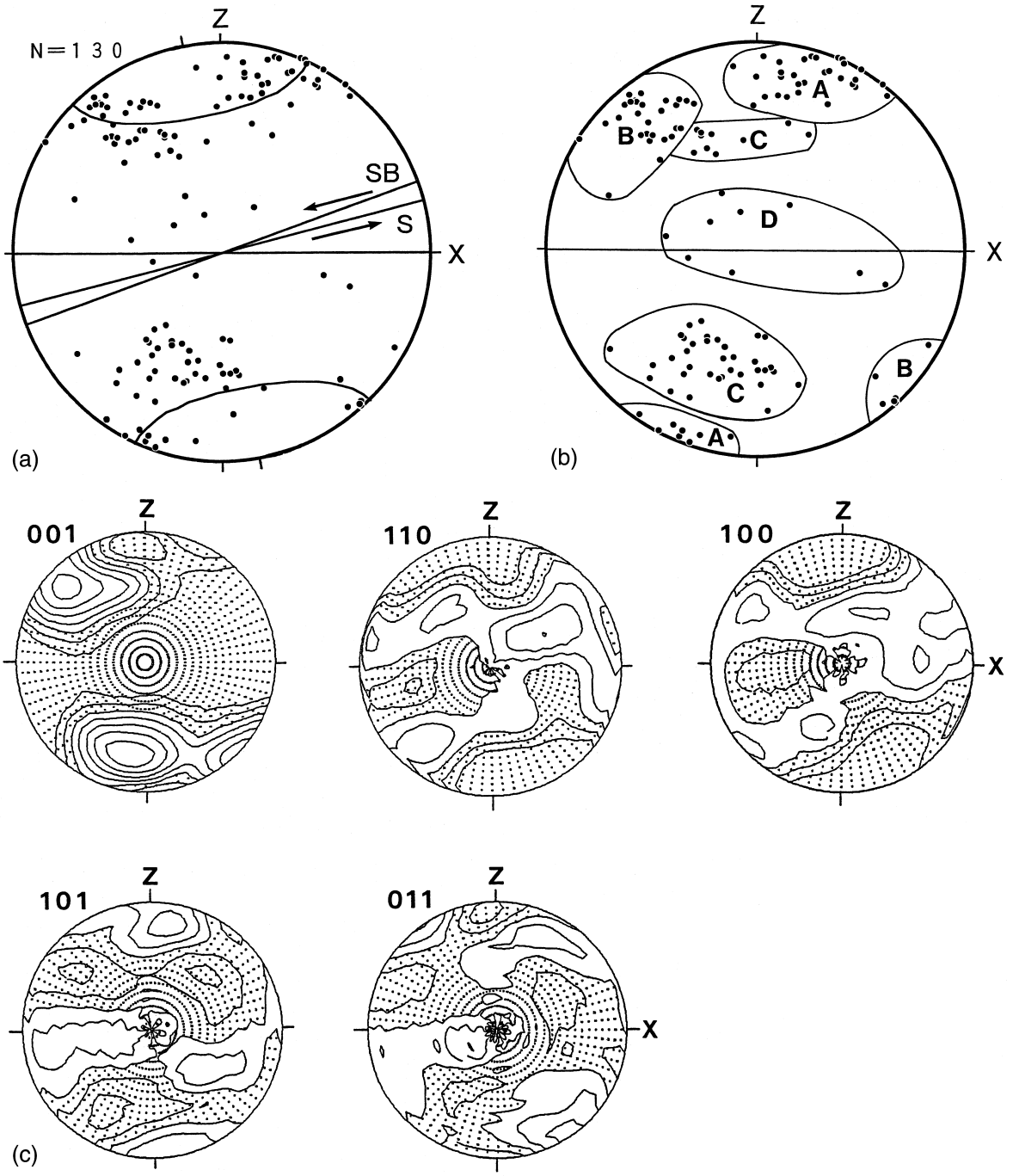

Fig. 2. Quartz texture in sample Sci 490. Upper-hemisphere and equal-area projection in the *X Z* plane. *X* and *Z* denote the elongation and shortening axes of finite strain, respectively. (a) Scatter diagram of the individual average host *c*-axis orientations. 130 host grains were analyzed. The 35° small circles which best approximate the *c*-axis fabric are shown by solid lines. The great circles denoted by *SB* and *S* indicate the average trace of shear bands and estimated bulk shear plane, respectively (see text). Arrows indicate the sense of shear. (b) Same as (a) but indicates orientation components A through D of the host *c*-axis orientations. (c) (001), (110), (100), (101) and (011) pole figures measured by neutron diffraction after Helming et al. (1994). Logarithmic contour intervals (0.5, 0.71, 1, etc. multiples of a random distribution). Dot pattern below 1 m.r.d.

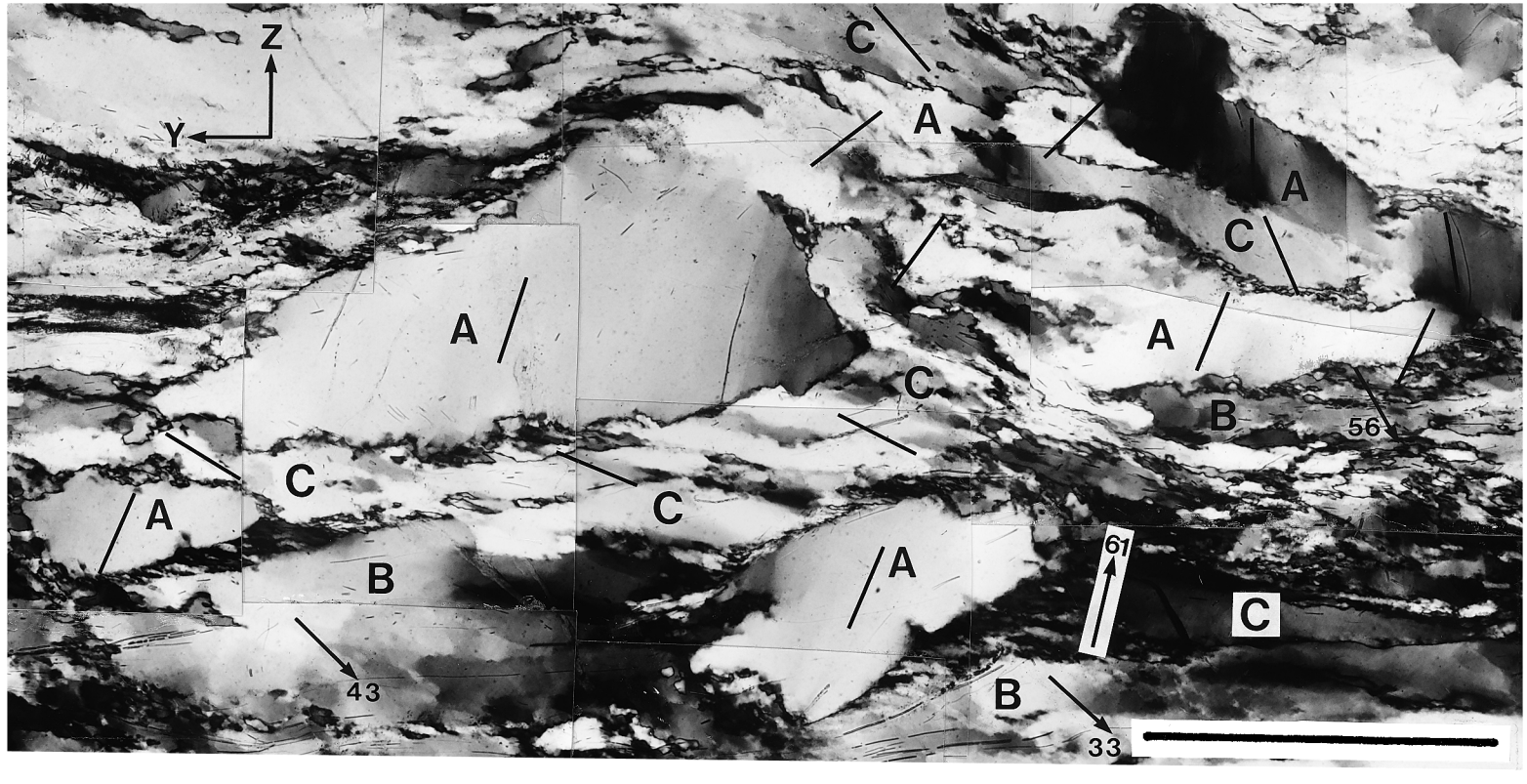

Fig. 3. Micrograph (crossed polarizers) in the *Y Z* section (orientations shown by arrows) showing deformation and recrystallization microstructures of host grains belonging to orientation components A through C (see text, denoted by A through C). Note that globular A-grains were separated from a single original grain and polygonized and partly recrystallized C-grains invaded the gaps. Some parts of the A-grains were rotated to favorable orientations for basal (0001) slip so that they were deformed extensively. The azimuth of *c*-axis orientation in each grain is shown by bars. For grains where the plunge of *c*-axis orientation exceeds 30º, the *c*-axis orientations are shown by arrows with the numbers indicating their plunges. Scale bar 0.5 mm.

3.2.2. Component B ('B-grains')

B-grains are generally highly stretched and can be called ribbon grains. Narrow kink bands (35–60 μm in width) whose boundaries are (sub-)parallel to the *c*-axis are pervasively developed in B-grains (Fig. 4). It is thus inferred that basal slip was dominant and B-grains were perhaps in the favorable orientations for basal slip during most of the non-coaxial strain history.

3.2.3. Component C ('C-grains')

C-grains are also stretched, similar to B-grains (Figs. 3 and 4). Even though kink bands with boundaries (sub-)parallel to the *c*-axis are also developed as in B-grains, inhomogeneous patchy and wavy extinction is more common in C-grains than in other differently oriented grains (Fig. 9). Subbasal deformation lamellae after Ave Lallement and Carter (1971) are sometimes found only in C-grains indicating the occurrence of basal slip.

3.2.4. Component D ('D-grains')

D-grains are mostly characterized by elongated kink bands (ca. 50–100 μm in width) whose boundaries are parallel to both the *c*-axis and the trace of foliation (Fig. 4), suggesting the dominant activation of basal slip. D-grains are slightly more deformed than A-grains, but less deformed than B- and C-grains, as is quantitatively analyzed below.

3.3. Microstructures of deformed host grains

In the analyzed quartzite sample, it is easy to trace the outline of A- and D-grains under a microscope because these grains are little and only partly recrystallized, respectively (Figs. 3 and 4). B- and C-grains are extensively (or moderately in some cases) recrystallized (Figs. 4 and 9) consisting of a polygonized (or kinked) core and a recrystallized mantle. As discussed below, recrystallization occurs by both subgrain rotation and grain boundary migration in the quartzite sample. In the case that recrystallization is moderate and dominantly occurring by subgrain rotation in both B- and C-grains, it can be possible to identify the outline of the shape of deformed original grains before recrystallization by tracing the continuity of crystallographic orientations in recrystallized grains under a microscope. This way we measured the length of long and short axes (denoted as a and b, respectively) and determined the diameter of equivalent circle ($\sqrt{ab}$, here referred to as the equivalent diameter) and aspect ratio (a/b) of deformed shape of host grains both in the XZ and YZ sections.

The aspect ratio has been analyzed as a function of *c*-axis orientation. The aspect ratio can be approximated as strain ratio both in the XZ and YZ sections, if the initial shape of detrital quartz grains is close to a sphere. The mean aspect ratios in different orientation components vary greatly: A 3.5, B 12.2, C 9.4 and D 4.6, and A 4.9, B 10.6, C 8.6 and D 5.6 in the XZ and YZ sections, respectively (Fig. 5). The aspect ratios of B- and C-grains are slightly but consistently higher in the XZ than in the YZ sections, and the *k*-value (Flinn, 1962) for these grains is inferred to be 0.01 (oblate shape).

It is clear from the detailed analysis of grain aspect ratios that B- and C-grains are much more strained than A- and D-grains, in other words there was a large plastic anisotropy. The plastic anisotropy is also clearly shown in both *c*-axis fabric diagrams from the XZ and YZ sections (Fig. 6) where the size of square symbols showing individual *c*-axis orientations is proportional to the value of the aspect ratio in each grain.

The individual equivalent diameter has also been analyzed as a function of *c*-axis orientation. The mean equivalent diameters of A-, B-, C- and D-grains are 536, 1609, 1427 and 802 μm in the XZ, and 745, 989, 1167 and 1544 μm in the YZ sections, respectively, indicating that A-grains are much smaller than the other differently oriented grains (Fig. 7). This is not necessarily due to a smaller original size of the A-grains, but rather indicates that some of A-grains are separated fragments of initially larger host grains which are dispersed into strongly deformed B- and C-grains (ductile matrix), as shown in Figs. 3 and 4. The fracturing of A-grains suggests that they were oriented in hard orientations during most of the non-coaxial strain history.

3.4. c-axis fabric and microstructures of recrystallized grains

As mentioned earlier, while A-grains are little recrystallized and D-grains are only partly recrys-

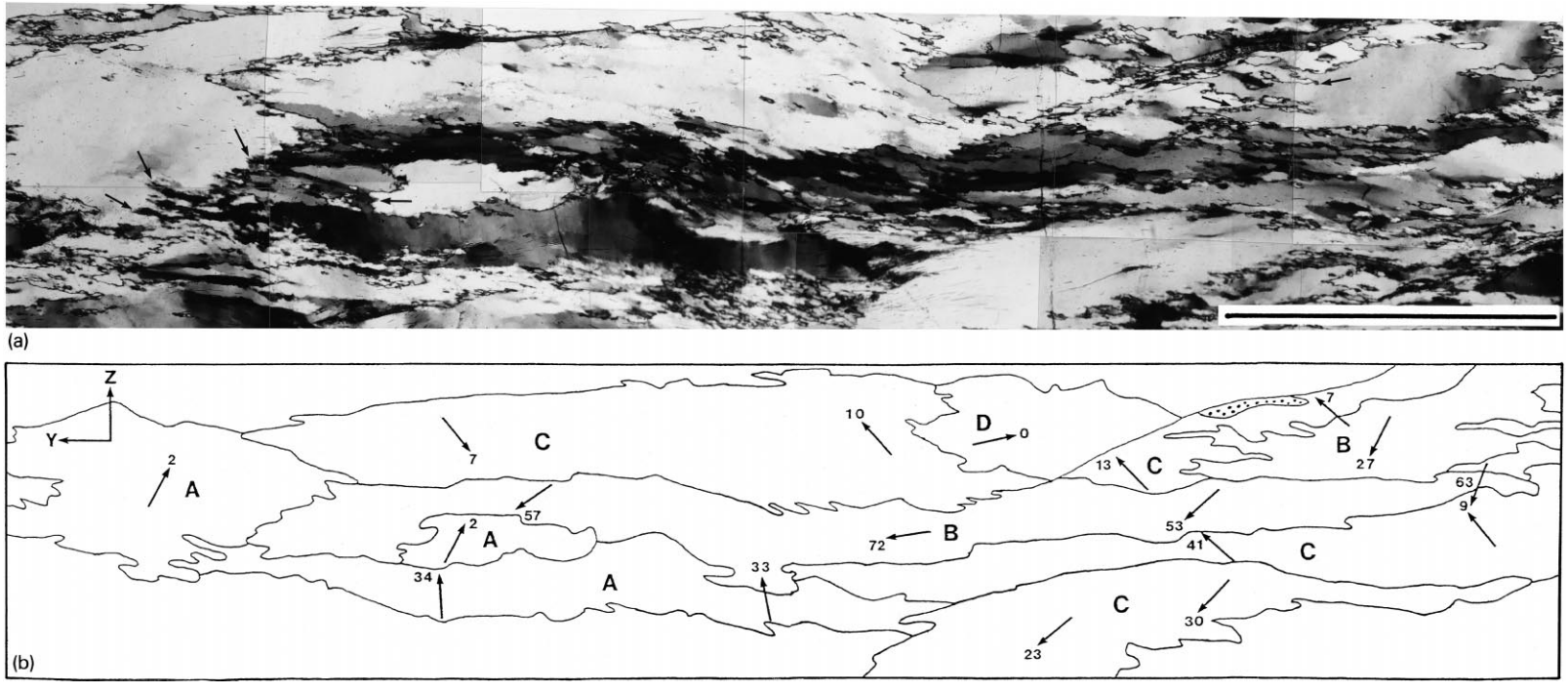

Fig. 4. (a) Micrograph (crossed polarizers) and (b) sketch (for the same area and magnification as (a)) in the *Y Z* section (orientations shown by arrows in (b)) showing deformation and recrystallization microstructures of host grains belonging to orientation components A through D (see text, denoted by *A* through *D* in (b)). Both B- and C-grains are highly deformed and extensively recrystallized. Kink bands parallel to both the *c*-axis and the trace of foliation are developed in a moderately deformed D-grain. Note that an A-grain at the left side is pulled apart, and recrystallized B-grains flow into the gap. Also note lobate or serrated shape of grain boundaries denoted by small arrows in (a), indicative of the occurrence of grain boundary migration. The *c*-axis orientation in each grain is shown by an arrow with the number indicating its plunge in (b). Dots in (b) denote muscovite. Scale bar in (a) 1 mm.

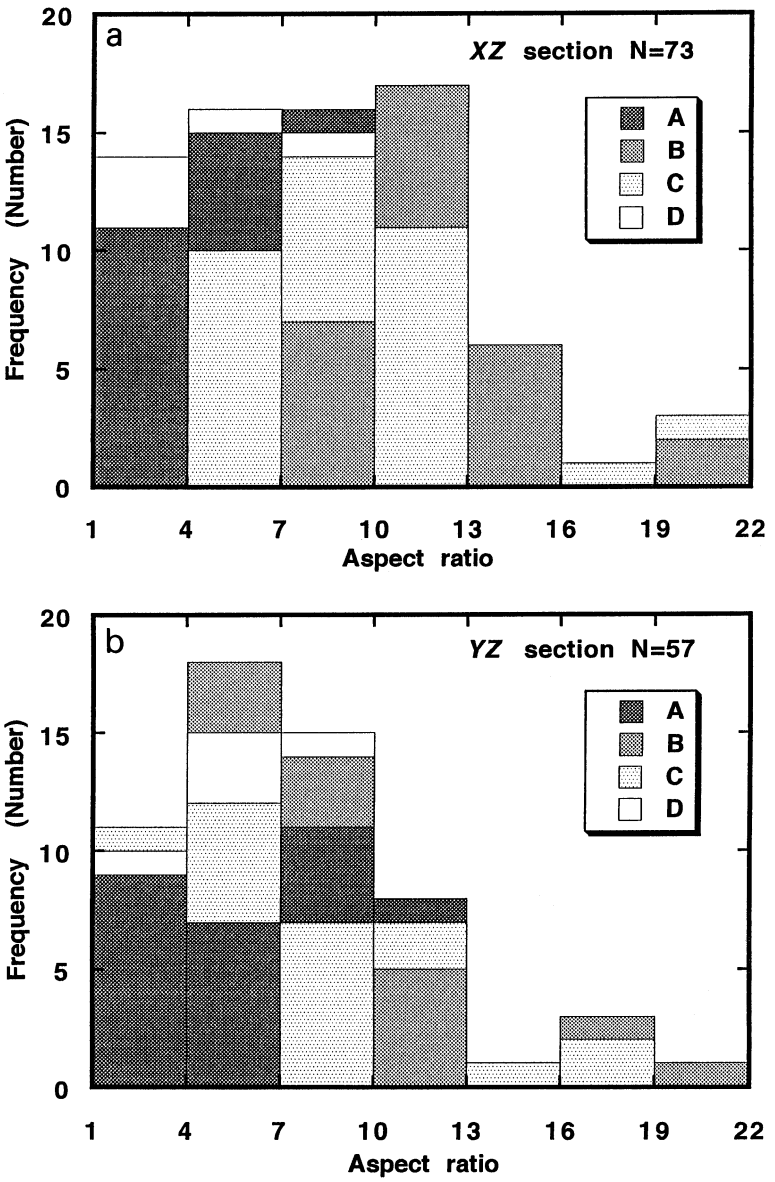

Fig. 5. Frequency distribution of aspect ratio of host grains represented separately for each orientation component A through D (see text). The number of analyzed host grains is 73 and 57 for the XZ and YZ sections, respectively. (a) XZ section. (b) YZ section.

tallized, both B- and C-grains are either moderately or extensively recrystallized. This confirms that the degree of dynamic recrystallization increased with increasing strain undergone by differently oriented grains.

Microstructures and LPOs of recrystallized grains can tell us the mechanisms of dynamic recrystallization. The composite *c*-axis fabric diagram from both host and recrystallized *c*-axis orientations in the quartzite sample is shown in Fig. 8a. Although the composite *c*-axis fabric does not differ greatly from the host *c*-axis fabric (Fig. 2a), it is more scattered. Furthermore, the density of the B-component is higher in the composite (also in the (0001)

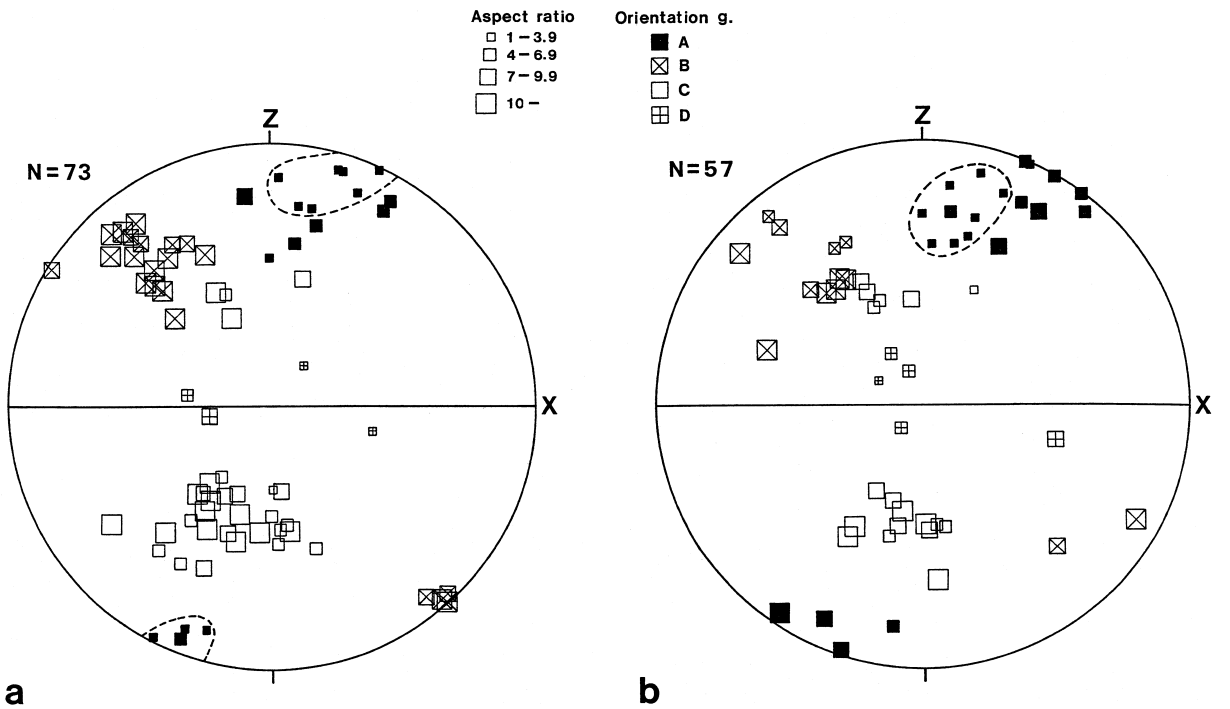

Fig. 6. Dependence of the aspect ratio of individual host grains on their *c*-axis orientations (plastic anisotropy). Upper-hemisphere and stereographic projection in the *XZ* plane. The aspect ratio is denoted by the size of square marks indicating individual host *c*-axis orientations. Each host *c*-axis orientation belongs to different orientation components A through D (see text) shown by different symbols. *X* and *Z* denote the elongation and shortening axes of finite strain, respectively. See text for the explanation of dashed lines. The number of analyzed host grains is 73 and 57 for the *XZ* and *YZ* sections, respectively. (a) *XZ* section. (b) *YZ* section (projected in the *XZ* plane).

pole figure by neutron diffraction, Fig. 2c) than in the host *c*-axis fabric, indicating the higher density of the B-component in the recrystallized *c*-axis fabric. The *c*-axis orientation distribution in recrystallized grains originating from some selected B- and C-grains is shown in Fig. 8b. From this figure, it is seen that although the *c*-axis orientations cluster around the host *c*-axis orientations, they are fairly scattered, particularly those in recrystallized grains originating from C-grains.

The *c*-axis orientation distribution in recrystallized grains originating from a C-grain was analyzed in detail (Fig. 9). First, note that the long axes of recrystallized grains are rotated clockwise by 10–30° from the *X*-axis about the *Y*-axis forming the oblique foliation indicative of a shear deformation with a top-to-the-northwest sense. Based on the *c*-axis fabric of recrystallized grains (Fig. 9b) (and also the recrystallized *c*-axis fabric shown in Fig. 8b), it can be shown that recrystallized grains are divided into two types. In the first type *c*-axis orientations of recrystallized grains are similar and continuous to the host *c*-axis orientations. In the second type *c*-axis misorientations from the host *c*-axis are large, mostly more than 50° and up to 90°. The former and latter types of recrystallized grains were presumably caused by subgrain rotation and grain boundary migration recrystallization with the formation of low- and high-angle grain boundaries, respectively.

The shape of high-angle boundaries of both deformed host and recrystallized grains is often extremely lobate or serrate indicating grain boundary migration (Fig. 4a and Fig. 9a). It seems that C- and D-grains were significantly consumed by the grain boundary migration of recrystallized grains oriented in B-directions (here referred to as recrystallized B-component). A common example is shown in Fig. 9, where the recrystallized B-component significantly grows at the expense of a C-grain by grain boundary migration.

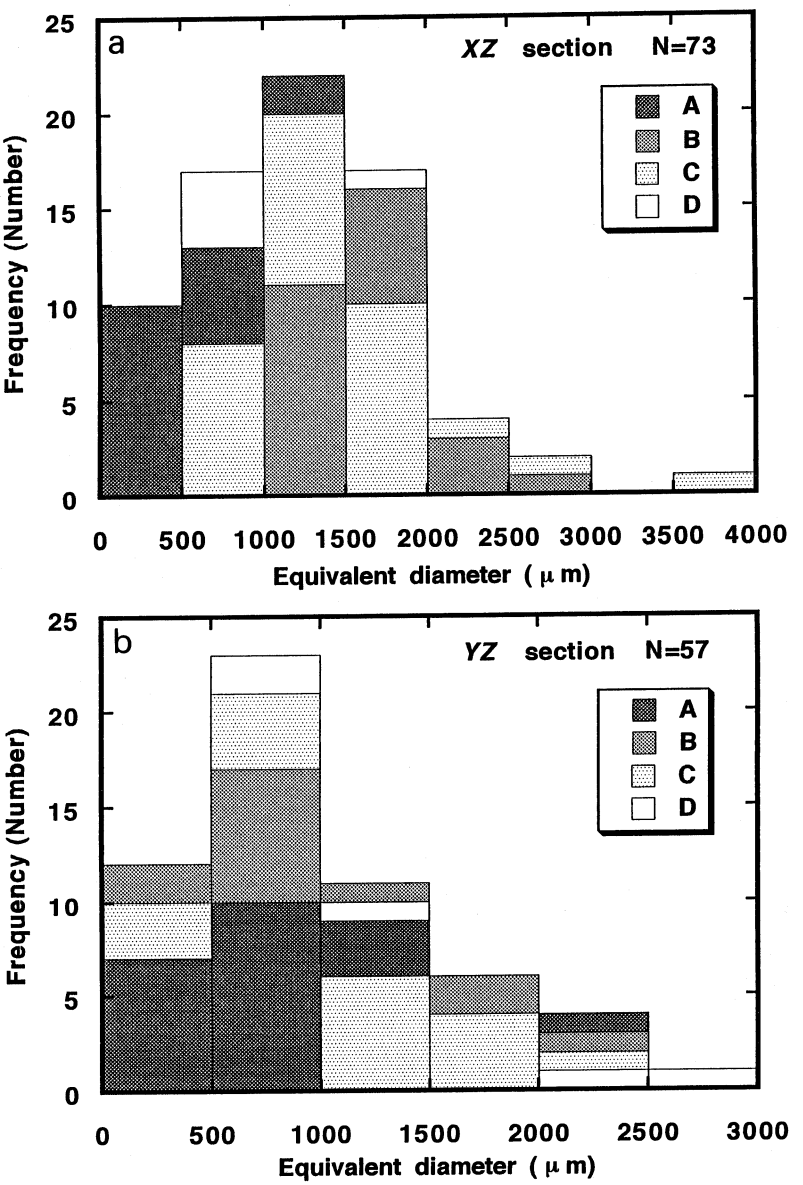

Fig. 7. Frequency distribution of equivalent diameter (see text) of host grains represented separately for each orientation component A through D (see text). The number of analyzed host grains is 73 and 57 for the *X Z* and *Y Z* sections, respectively. (a) *X Z* section. (b) *Y Z* section.

4. Simulation of *c*-axis fabric development in quartzite by a deformation-based model of recrystallization

4.1. Model

The complex mutual influence of anisotropy, LPO, plastic deformation and recrystallization of real polycrystalline materials has been investigated with polycrystal plasticity models (Kocks et al., 1998). A real polycrystal deforms maintaining local stress equilibrium and strain compatibility, which is achieved through the development of intergranular and intragranular heterogeneities (i.e. variation of stress and strain from grain to grain and within grains, respectively). The viscoplastic self-consis-

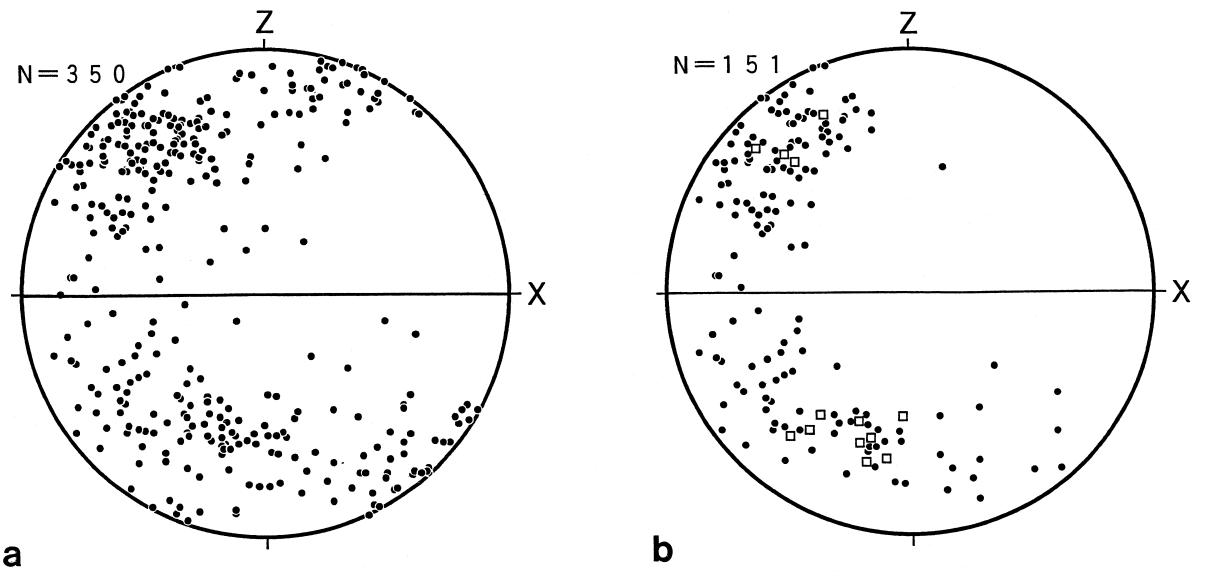

Fig. 8. (a) The composite *c*-axis fabric from both host and recrystallized *c*-axis orientations (the number of measurement is 350), and (b) the *c*-axis fabric in recrystallized grains from selected four B-grains and nine C-grains (the number of measurement is 151). Open squares in (b) denote the *c*-axis orientations of host grains. Upper-hemisphere and equal-area projection in the *XZ* plane. *X* and *Z* denote the elongation and shortening axes of finite strain, respectively.

tent (VPSC) formulation (e.g. Molinari et al., 1987; Lebensohn and Tomé, 1993) captures some aspects of this heterogeneity by allowing stress and strain rate in the grains to vary, depending on crystal orientation. The VPSC model basically considers each grain of the polycrystal as a viscoplastic inclusion deforming in a viscoplastic homogeneous effective medium having the average properties of the polycrystal. The model has been applied to hexagonal metals with similarity to quartz (Lebensohn and Tomé, 1994; Lebensohn et al., 1996) as well as many minerals (Wenk, 1999).

Based on the assumption that the stored strain energy provides the driving force for recrystallization, Wenk et al. (1997) proposed a deformation-based recrystallization model for low-symmetry materials, which has been implemented within the formulation. In the model, highly strained grains are likely to recrystallize by nucleation or to be replaced by grain boundary migration recrystallization of less deformed neighbor grains. Thus, the dynamic recrystallization texture is due to a balance between nucleation and boundary mobility that makes a grain shrink or grow. In the model nucleation occurs at a rate that is proportional to the local strain rate after a grain attains the threshold value of strain. It is assumed that the crystallographic orientation of nucleated grain is the same as that of the host grain. Therefore, the nucleation process in the model is similar to subgrain rotation recrystallization in real materials. In the model the stored strain energy of the nucleus which gradually replaces the host, is set to zero until the nucleus reaches a certain size, at which point the nucleus starts to harden again. The strain energy is calculated assuming a linear hardening law. If the stored strain energy of a grain is lower than the average strain energy in the polycrystal, it grows; if it is higher, it shrinks by grain boundary migration. The relative grain volume after each strain increment is calculated from the strain energy difference and boundary mobility.

The recrystallization simulations have been in good agreement with previously unexplained texture features observed in experimentally and naturally deformed rocks. For example recrystallized halite deformed in extension displays a (100) component in the inverse pole figure that corresponds to the most highly deformed grains (Wenk et al., 1997). In recrystallized quartz mylonites a conspicuous *c*-axis maximum oriented in the intermediate axis of finite

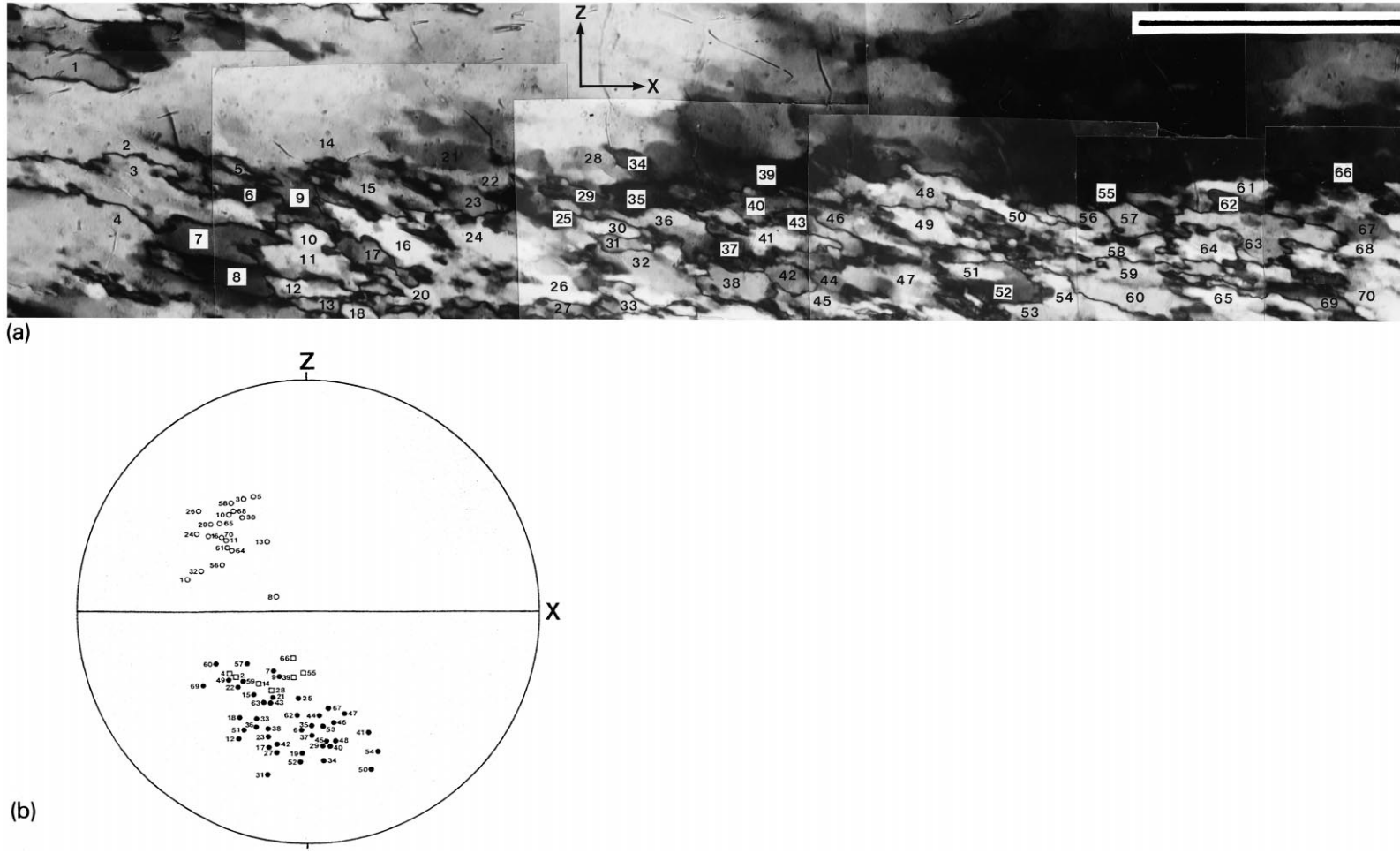

Fig. 9. Dynamic recrystallization in a selected C-grain. (a) Micrograph (crossed polarizers) in the *X Z* section (orientations shown by arrows). The numbers indicate each part in the host and recrystallized grains. Scale bar is 0.2 mm. (b) Upper-hemisphere and stereographic projection in the *X Z* plane of *c*-axis orientations in host and recrystallized grains from the C-grain. The numbers correspond to each part in the host and recrystallized grains shown in (a). Open squares denote host grains. Recrystallized grains denoted by solid and open circles were perhaps developed by subgrain rotation and grain boundary migration recrystallization, respectively. See text for further explanations.

strain is often observed. Also here this corresponds to the most highly deformed grains which nucleate and replace less deformed grains (Wenk et al., 1997). An enigmatic maximum at high-angle positive rhombs in inverse pole figures of calcite deformed in compression and displaying an increase in grain size could be interpreted as due to growth of the least deformed grains (Lebensohn et al., 1998). Simulations of Wenk and Tomé (1999) predicted the [100] maximum in the shear direction observed in experimentally and naturally deformed and recrystallized olivine.

4.2. Results: comparison of natural data and simulated results

The natural fabric contains information about strain path and microscopic deformation mechanisms that were active during the deformation process. The VPSC model is used here to assess which active slip systems are compatible with the measured natural *c*-axis fabric. In the simulations we assumed that the active slip systems during deformation were essentially basal$\langle a\rangle$, pyramid$\langle a\rangle$ and pyramid$\langle a+c\rangle$ slip systems (here quartz crystal is treated as hexagonal), and three different combinations (α, β and γ) were investigated (Table 1). It was determined in the quartzite that basal slip was dominant because of the frequent occurrence of subbasal lamellae in C-grains and the orientation relationship between the host *c*-axis and kink band boundaries in all of the differently oriented grains. The pyramid$\langle a\rangle$ slip has been recently documented to be important at greenschist facies conditions by the misorientation analysis between recrystallized grains (or subgrains) (e.g. Lloyd and Freeman, 1994). In the VPSC model (or other polycrystal plasticity models), some activity of pyramid$\langle a+c\rangle$ slip is always required to accommodate the shortening (or elongation) parallel to the *c*-axis in quartz (e.g. Takeshita and Wenk, 1988). The activation of pyramid$\langle a+c\rangle$ slip has also been documented experimentally in naturally deformed quartz (Fliervoet and White, 1995).

The stress exponent was taken as 3 for the simulations. Simulations for deformation and dynamic recrystallization which follows the deformation were performed for an intermediate strain path between uniaxial shortening and simple shear, although the observed *oblate* deformed grain shape is not ideally reproduced by such a strain path. The velocity gradient tensor (L_{ij}) for 2.5% shear strain increment which we chose for the calculation is described as follows.

$$L_{ij}=\begin{pmatrix}0.025 & -0.05 & 0.0\\ 0.0 & -0.0125 & 0.0\\ 0.0 & 0.0 & -0.0125\end{pmatrix} \quad (1)$$

In all cases we started with 250 randomly oriented and equally sized orientations, and the deformation was carried out up to 1.0 shear strain (40 steps). All the fabric diagrams represented in the paper were obtained from the orientation distribution using the Berkeley texture package (Wenk et al., 1998).

Fig. 10 illustrates the evolution of the deformation *c*-axis fabric for conditions of basal$\langle a\rangle$ and pyramid$\langle a\rangle$ slip equally easy (model β). As in previous simulations a broad girdle develops with a (0001) maximum near the shear plane normal but slightly rotated against the sense of shear (Lister and Williams, 1979; Wenk et al., 1989). The simulated *c*-axis fabric is more or less similar with correlative components to the natural *c*-axis fabric. The *c*-axis fabric patterns are similar for all three models α, β and γ which are shown together with the overall deformation of individual grains and the shear due to

Table 1
Slip systems for quartz (treated as hexagonal crystal), number of systems in each family (*n*), critical resolved shear stress (CRSS) ratios relative to basal slip and hardening per unit strain used in the polycrystal plasticity simulations

Slip system	Abbreviation	*n*	α	β	γ	Hardening per unit strain
$(0001)\langle\bar{1}2\bar{1}0\rangle$	basal$\langle a\rangle$	3	1	1	1	0.05
$\{10\bar{1}0\}\langle\bar{1}2\bar{1}0\rangle$	prism$\langle a\rangle$	3	5	5	5	0.05
$\{10\bar{1}1\}\langle\bar{1}2\bar{1}0\rangle$	pyramid$\langle a\rangle$	6	1.5	1	0.5	0.05
$\{10\bar{1}1\}\langle\bar{1}\bar{1}23\rangle$	pyramid$\langle a+c\rangle$	12	2	2	2	0.05

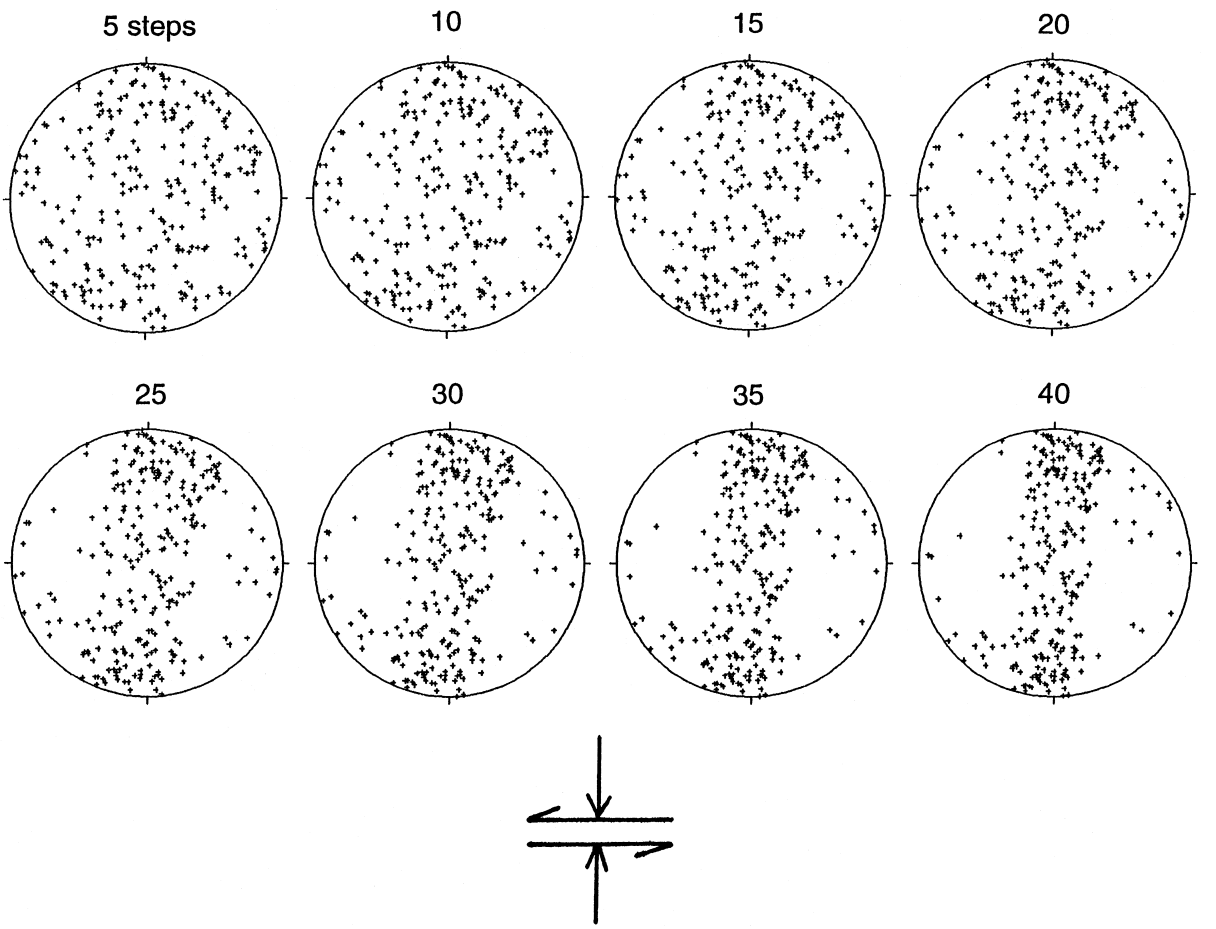

Fig. 10. VPSC deformation simulation of *c*-axis fabric development for model quartzite β (Table 1) deformed in combined uniaxial shortening and simple shear. The shear plane, the shear direction and the sense of shear are indicated by arrows. The shortening direction is perpendicular to the shear plane, which is also indicated by arrows. Deformation step is 2.5% shear strain. Equal area projections. 250 orientations.

basal slip (Fig. 11). Fig. 12 shows the activity of different families of slip systems with increasing shear strain. It is shown from Fig. 12 that pyramid$\langle a \rangle$ slip is as active as, and more active than basal$\langle a \rangle$ slip for model α, and models β and γ, respectively. While in the previous simulation (model α of Wenk et al., 1989) where the CRSS of pyramid$\langle a \rangle$ slip is three times as high as that of basal$\langle a \rangle$ slip, the C-component cannot be created, in all of the present models the C-component is distinct (Fig. 11), suggesting a significant activity of pyramid$\langle a \rangle$ slip in the quartzite sample.

It is clear from these calculations that grains with *c*-axes near the shear plane normal (corresponding to B-grains in the natural texture) are most heavily deformed with additional highly deformed grains closer to the Y-axis (C-grains). Grains with *c*-axes rotated against the sense of shear (A-grains) are significantly harder than B-grains. Grains with *c*-axes oriented around the Y-axis (D-grains) are moderately deformed for model α, but highly deformed for models β and γ. Since B- and C-grains are more deformed than D-grains in the quartzite sample, model α best approximates the plastic anisotropy. Overall, for model α 'soft' highly deformed grains correspond to grains with significant basal slip (Fig. 11a,b).

During deformation by slip crystals rotate in the

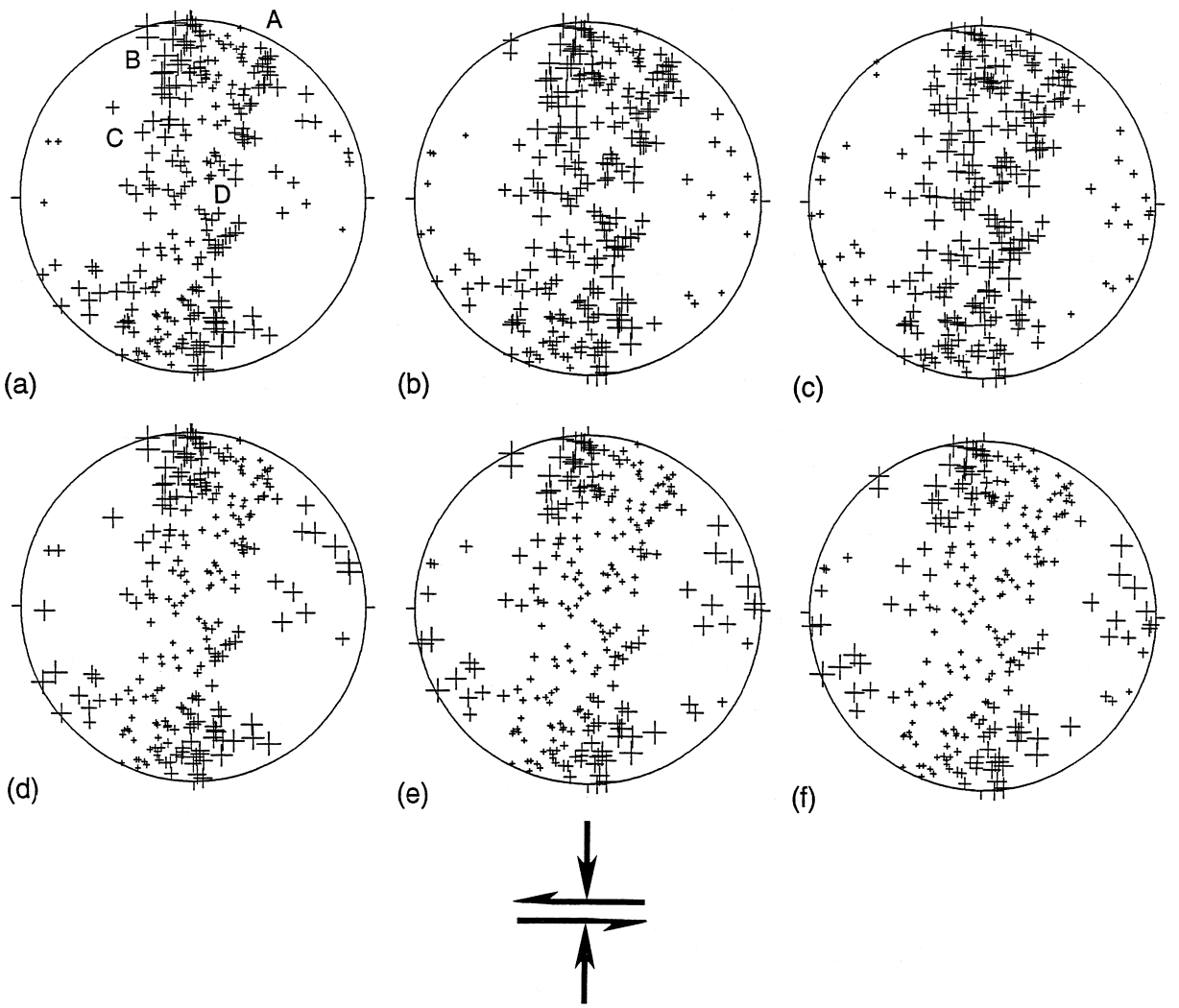

Fig. 11. VPSC deformation simulation of *c*-axis fabric development as in Fig. 10 but for model α (a and d), β (b and e) and γ (c and f) (Table 1) after 30 steps; *c*-axis fabric diagram with symbol size illustrating relative equivalent deformation of different orientations (a–c) and the relative activity of basal slip during the 30th step (d–f). Orientation components A through D are indicated by labels in (a). See Fig. 10 for explanation of arrows.

VPSC framework due to a vorticity caused by shear on slip systems, to rigid body rotation of the sample and due to a relative rotation of the equivalent polycrystal (Kocks et al., 1998). Different orientations rotate differently. Fig. 13 shows *c*-axis rotation trajectories for nine orientations with symbol sizes indicating increased deformation. It can be seen that most rotations are in the sense of shear. Rotations are large for grains near the shear direction, while rotations for grains near the normal orientation of shear plane and the *Y*-direction are small. It should be noted that two crystals with the same *c*-axis but different *a*-axis orientations behave very differently. For example some grains with *c*-axes near the shear direction are favorably oriented for basal slip and undergo large rotations such as an example illustrated in Fig. 13, whereas others do not deform and hence do not rotate appreciably.

Dynamic recrystallization was initiated after 30 steps (shear strain of 0.75 corresponding to *c*-axis patterns illustrated in Fig. 11). Fig. 14 shows the *c*-axis texture evolution for the three models for

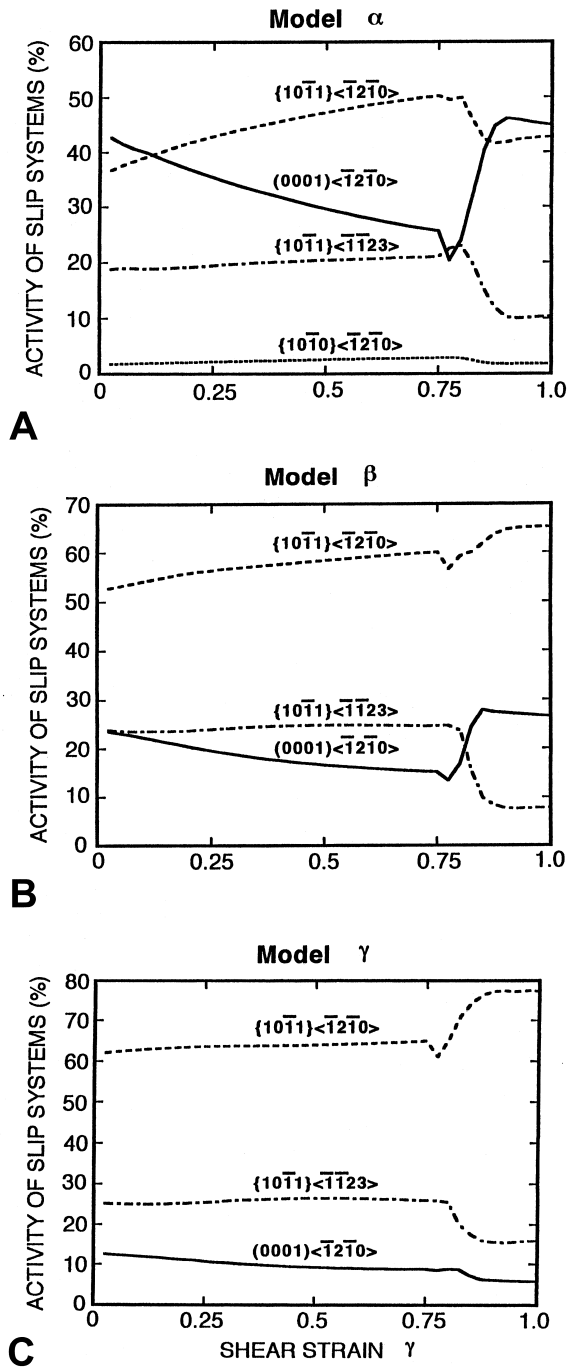

Fig. 12. VPSC deformation and recrystallization simulation for model quartzite α, β and γ (Table 1). Relative activity (%) of slip systems for the different models as a function of shear strain. For models β and γ, the activity of $\{10\bar{1}0\}\langle\bar{1}2\bar{1}0\rangle$(prism$\langle a\rangle$) slip is negligible (less than 0.5%).

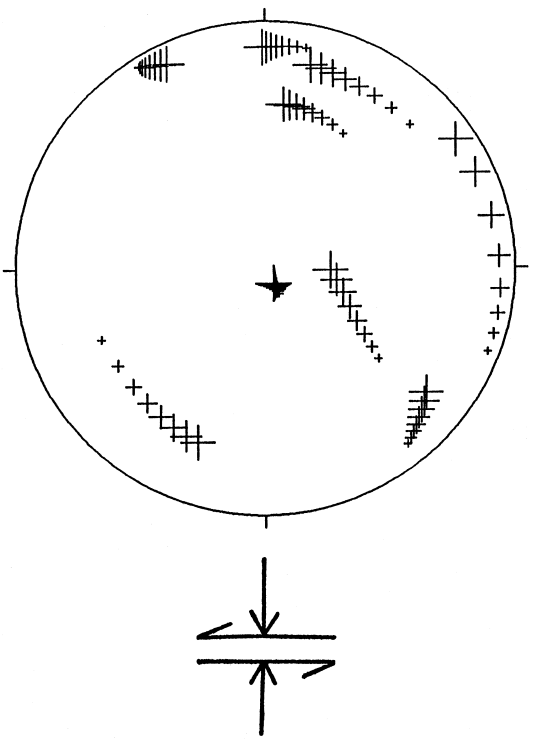

Fig. 13. Rotation trajectories for *c*-axes of nine grains during deformation for model quartzite β. The symbol size is proportional to the overall grain deformation. Equal-area projection. See Fig. 10 for explanation of arrows.

steps 28, 30, 32 and 34. In these figures, +-symbols identify old grains, −-symbols stand for newly nucleated grains. The symbol size is proportional to the grain volume (grain size). In all three models many grains disappear and the final texture is dominated by grains with *c*-axes near the shear plane normal (B-grains) if basal slip is easier (model α, Fig. 14a), and grains at intermediate directions (C-grains) if pyramid$\langle a\rangle$ slip is easier (model γ, Fig. 14c). If basal and pyramid$\langle a\rangle$ slip are equally easy, the final texture is dominated by both B- and C-grains (model β, Fig. 14b). The results also interpret the changes in the activity of different families of slip systems with increasing strain after the onset of recrystallization (i.e. increase of activity of basal, basal and pyramid$\langle a\rangle$ and pyramid$\langle a\rangle$ slip for models α, β and γ, respectively, in Fig. 12). The final texture components correspond to 'easy slip' orientations with the slip directions of the major slip system oriented

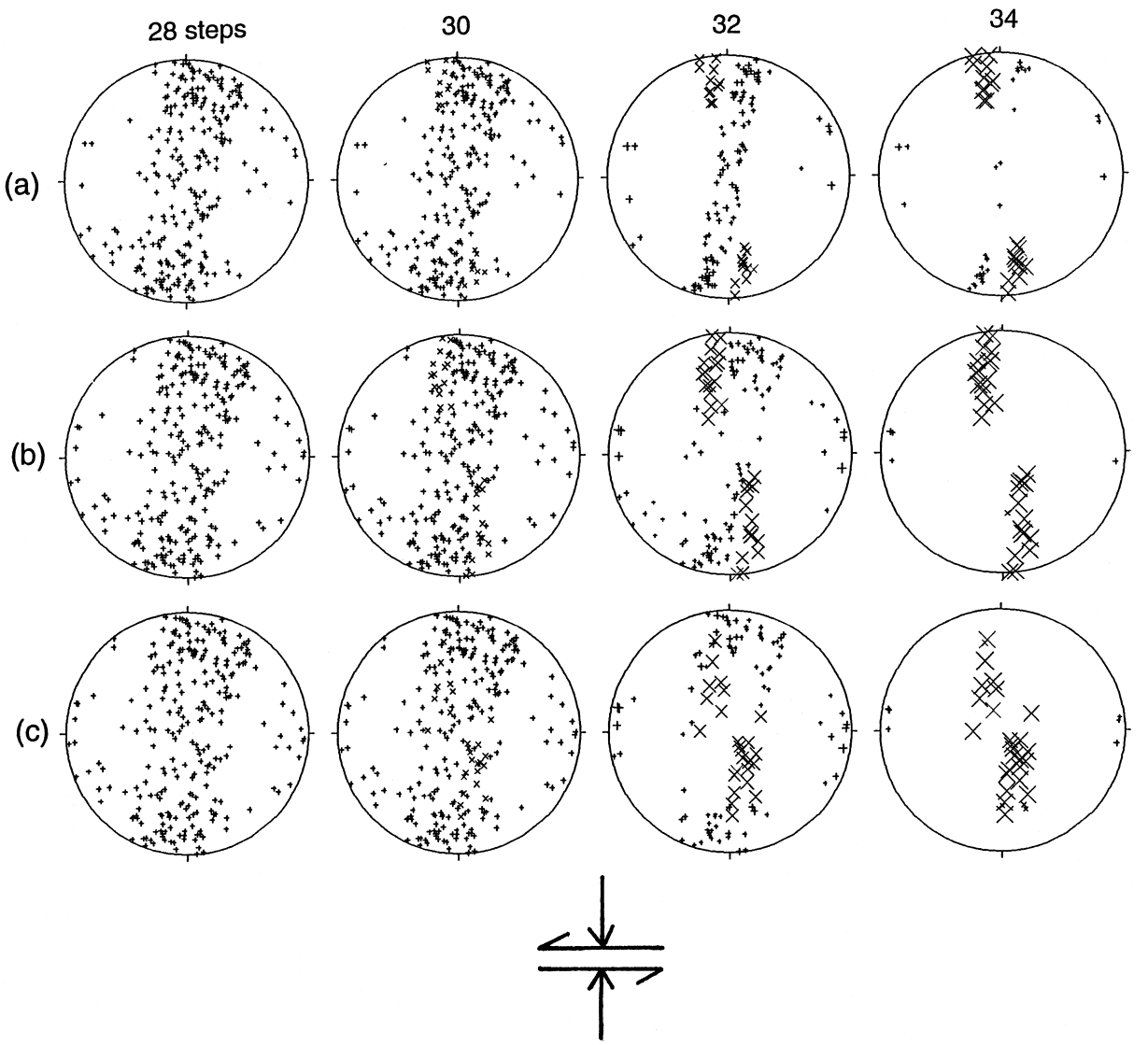

Fig. 14. Simulation of *c*-axis fabric development for combined uniaxial shortening and simple shear in model α (a), β (b) and γ (c) quartzite. The fabric development is caused by both intracrystalline slip and dynamic recrystallization (i.e. nucleation and growth). Steps 28, 30, 32 and 34 are shown, recrystallization starts after step 30, the texture illustrated in step 34 does not change appreciably with further straining. Equal-area projection. The symbol + indicates old grains, × grains that have nucleated at least once; the size of the symbols is proportional to the grain volume.

parallel to the macroscopic shear direction and the slip plane parallel to the shear plane. These orientations are special for simple shear deformation in a self-consistent framework because in such a texture a single crystal deforms basically in a 'single crystal' on a single slip system with no rotation. During dynamic recrystallization such a component remains stable to large strains as has been shown for quartz (e.g. Schmid et al., 1981), olivine (Wenk and Tomé, 1999) and calcite (Kunze et al., 1998).

In the model changes occur rather rapidly after the onset of recrystallization and in only eight steps an equilibrium dynamic recrystallization texture establishes. This is largely due to the selection of

the recrystallization parameters for boundary migration velocity and nucleation rate relative to strain rate. The texture in the natural sample investigated here corresponds best with the simulated textures in early stages of recrystallization (steps 31–33). In accordance with microstructural evidence, recrystallization parameters were chosen such that nucleation dominates over growth and in the end only nucleated grains persist. Whereas deformation textures are similar for different choices of critical stress ratios, there are distinct differences for dynamic recrystallization. The best agreement with the natural texture where the recrystallized B-component is predominant is obtained for conditions of easier basal than pyramid$\langle a \rangle$ slip (model α, Fig. 14a). If prism$\langle a \rangle$ slip becomes important, the *c*-axis maximum shifts to *Y* (Wenk et al., 1997), corresponding to textures observed in high-temperature quartz mylonites. It is an indication that in the sample Sci 490 prism$\langle a \rangle$ slip is subordinate.

5. Discussion

5.1. The sense of rotation of the host c-axis fabric skeleton relative to coaxial deformation

In the analyzed quartzite sample, the top-to-the-northwest sense of shear is obvious based on both the arrangement of shear bands and the internal asymmetry of the *c*-axis fabric. It agrees with the field evidence for emplacement of the Bergell granite in a largely solid state from the south over underlying Pennine nappes which contain the quartzite sample described in this investigation (Wenk, 1973). In this study, we have compared the sense of rotation of the host *c*-axis fabric relative to coaxial deformation in the natural sample with that in simulations. The simulated *c*-axis fabric for combined uniaxial shortening and simple shear is obviously rotated against the sense of shear (Fig. 10), while the natural *c*-axis fabric is apparently rotated by 10° with the sense of shear about the *Y*-axis. Note, however, that while the natural *c*-axis fabric is plotted in the frame of finite strain, the simulated *c*-axis fabric is plotted in the frame of the shear plane. Hence, we have to infer the orientation of the bulk shear plane in the natural quartzite for a proper comparison of the rotation sense between the natural and simulated *c*-axis fabrics. A crude estimate on the orientation of the bulk shear plane in the natural quartzite is given below.

Assuming that the *X*-axis is exactly parallel to the finite elongation direction and the shear strain (γ) is 4 (which yields a strain ratio of ca. 17 for simple shear) in the *XZ* section, the angle θ between the finite elongation axis and shear plane is calculated as 14° for the simple shear based on the equation ($\tan 2\theta = 2/\gamma$) and indicated as *S* in Fig. 2a. The angle θ exceeds the rotation angle of the small circle *c*-axis fabric with the sense of shear (10°). Hence, it may be concluded that the *c*-axis fabric skeleton is rotated against the sense of shear relative to coaxial deformation in the natural quartzite, although the actual angle θ could be significantly lower than 14° for combined uniaxial shortening and simple shear.

Some authors reported natural quartz simple shear *c*-axis fabrics (asymmetric crossed girdles, not a single girdle) which are rotated against the sense of shear relative to coaxial deformation viewed in the frame of shear plane (e.g. Brunel, 1980; Takeshita and Ise, 1994). Furthermore, the *c*-axis fabric skeletons at low strains in experimentally sheared quartzite (Dell' Angelo and Tullis, 1989) and quartz analogue (norcamphor, Herwegh and Handy, 1996) are consistently rotated against the sense of shear relative to coaxial deformation, where grain boundary migration recrystallization is not significant. Considering the complex strain paths and difficulty for the identification of the bulk shear plane in naturally deformed quartzites, it would be safe to conclude that the simple shear *c*-axis fabric skeleton formed by intracrystalline slip alone is rotated *against* the sense of shear relative to coaxial deformation.

5.2. Difference between the host and recrystallized c-axis fabrics: possible effect of dynamic recrystallization on the fabric development

Compared with the host *c*-axis fabric (Fig. 2a) where the *c*-axis orientations are concentrated in the narrow zones along the fabric skeleton, both the composite *c*-axis fabric from all the host and recrystallized *c*-axis orientations (Fig. 8a) and the *c*-axis fabric in recrystallized grains (Fig. 8b, Fig. 9b) are fairly scattered. The composite *c*-axis fabric skeleton

is reasonably approximated as asymmetrical small circles recognizable in the host *c*-axis fabric skeleton. The diffuse nature of the *c*-axis fabric in the recrystallized grains perhaps resulted from subgrain rotation recrystallization. On the other hand, the B-component is more dominant in the recrystallized than in the host *c*-axis fabric. The feature could be attributed to the oriented nucleation and growth of the B-component by grain boundary migration (also see Fig. 9).

It has recently been shown by simple shear deformation experiments of a quartz analogue (norcamphor) that with increasing strain the *c*-axis fabric is transformed from asymmetric crossed girdles (formed at shear strain $\gamma = 2$ to 4) through a single girdle (formed at $\gamma = 6$) into two discrete maxima (formed at $\gamma = 8$ to 10) which are oriented perpendicular to the bulk shear plane and in the intermediate strain (*Y*) axis, respectively (Herwegh and Handy, 1996). The fabric transition has been attributed to the increasing importance with increasing strain of grain boundary migration versus glide-induced vorticity and subgrain rotation. Since the final orientation components of the *c*-axes are favorable for the activation of basal and prism⟨*a*⟩ slip, the soft grains seem to have grown at the expense of neighboring hard grains by grain boundary migration as strain increased.

LPOs in polycrystals are formed by a few tens of percent of strain, and the individual crystallographic axis does not rotate much with further increasing strain relative to the fixed coordinates (i.e. the finite strain axes for coaxial deformation, and the shear plane for non-coaxial deformation without spinning) (e.g. Lister and Hobbs, 1980; Wenk et al., 1989). In fact, the present model suggests that the orientation components near the shear plane normal (A- and B-grains) and in the *Y*-axis (D-grains) are largely comprised of grains that are already initially close to these orientations, rather than grains that have rotated into these orientations (Fig. 13). Therefore, it is suggested in the present sample that A- and D-grains, unfavorably oriented for basal slip (hard grains), and B-grains favorably oriented for it (soft grains) remained close to these orientations during the deformation to large strains. Hence, the hardest orientation (i.e. that of the least deformed A-grains which are circled in Fig. 6) is roughly correlated with the compression direction with respect to the shear plane at large strains.

C-grains are less favorably oriented for basal slip than B-grains, but favorably oriented for harder pyramid⟨*a*⟩ slip in the framework of shear deformation discussed above. The fact that C-grains are slightly less deformed than B-grains suggests that these grains were mostly deformed by harder pyramid⟨*a*⟩ slip irrespective the occurrence of subbasal lamellae. Microstructural evidences suggest that both C- and D-grains were significantly consumed by the recrystallized B-component which nucleated and grew in the former grains (Fig. 9). Therefore, in the quartzite sample, softer grains for basal slip grew significantly at the expense of the harder grains by grain boundary migration. The conclusion is consistent with the result from the simple shear experiments on a quartz analogue (norcamphor) by Herwegh and Handy (1996), but opposite to deformation experiments on quartzite in regime I by Gleason et al. (1993) where the hard grains dominate the recrystallized *c*-axis fabric.

It can be inferred that the present asymmetric small circle *c*-axis fabric is ultimately transformed with increasing strain to a *c*-axis fabric dominated by orientations favorable for basal slip only (i.e. a single maximum perpendicular to the bulk shear plane). Such a single maximum *c*-axis fabric perpendicular to the shear plane (note that the *c*-axis maximum is rotated *with* the sense of shear viewed in the frame of finite strain) is observed in both experimentally sheared quartzite under low-temperature conditions (Dell' Angelo and Tullis, 1989) and naturally sheared quartz schists under greenschist facies conditions from the Sambagawa metamorphic belt (Tagami and Takeshita, 1996), where dynamic recrystallization is extensive. Hence, it is concluded that the commonly observed *c*-axis maximum near the *Z*-axis, rotated with the sense of shear, in natural quartzite sheared under greenschist conditions can be attributed to the growth of soft orientations at the expense of hard orientations for basal slip at large strains.

5.3. Some limitations in the current model of dynamic recrystallization

The deformation-based model of dynamic recrystallization can predict the essential textural and

microstructural features in the naturally deformed quartzite sample and therefore helps in the interpretation of the deformation history. Of particular significance are orientation-dependent strain magnitude (plastic anisotropy) and increasing degree of dynamic recrystallization with increasing strain undergone by differently oriented host grains. Also the model explains the observed 'easy slip' orientation as a stable component for dynamic recrystallization in shear deformation. However, there are some critical flaws in the current model, which will be discussed below.

In the current model, it is assumed that the crystallographic orientations of recrystallized (new) grains are the same as those of host grains. As a result, the recrystallized fabric is the same as some components of the deformation fabric, but the volume of different components changes due to concurrent grain boundary migration. In the real quartzite sample, however, recrystallization proceeds by subgrain rotation and grain boundary migration with the formation of low- and high-angle grain boundaries, respectively. Accordingly, the current model fails to predict the observed dispersion of the deformation fabric. This could be easily introduced by increasing the number of grains and by applying some spreading function during the nucleation event.

Another consideration is preferred nucleation in specific high-angle misorientations such as lattice coincidence misorientations (e.g. McLaren, 1986) observed in some metals. In order to include such features it must be first established for quartz (e.g. by EBSD misorientation analysis) if such misorientations exist for quartz or if some nuclei form in arbitrary orientations, unrelated to the host crystal. In the case that misorientations are important in a particular system, it would be more natural to advance to an approach which takes the polycrystal grain topology into account (e.g. the self-consistent n-site model of Canova et al., 1992, or finite element methods as described by Dawson and Beaudoin, 1998) to allow for selective nucleation and specific boundary migration.

6. Conclusions

(1) In the quartzite sample sheared under greenschist facies conditions (with basal $(0001)\langle a\rangle$ and likely pyramid $\{10\bar{1}1\}\langle a\rangle$ slip), an asymmetric small circle *c*-axis fabric about the finite shortening (*z*-) axis with a small half opening angle (35°) is developed consisting of four orientation components which are represented by host grain *c*-axis orientations (referred to as A, B, C and D): A and B are at high angles to the foliation plane, displaced against and with the sense of shear, respectively; C is in an intermediate direction between the Y- and Z-axes of finite strain, and D forms a subsidiary concentration around the intermediate strain (Y) axis. B- and C-grains are favorably oriented for basal$\langle a\rangle$ and pyramid$\langle a\rangle$ slip, respectively, and are strongly deformed, while both A- and D-grains are unfavorably oriented for the slip systems and are little or moderately deformed. Some of the A-grains are even fractured. The strong plastic anisotropy in the sample can be well simulated by the VPSC (viscoplastic self-consistent) model, but not by the model of Taylor (1938) which assumes homogeneous deformation.

(2) The 3-D strain ratios in differently oriented host grains which were estimated from the aspect ratios in both the XZ and YZ sections indicate that the magnitude of strain increases in the sequence of A-, D-, C-, B-grains. While A-grains are little recrystallized and D-grains are only partly recrystallized, B- and C-grains are extensively recrystallized, supporting the concept of strain-induced dynamic recrystallization.

(3) The microstructural appearances indicate that harder C- and D-grains were significantly consumed by the grain boundary migration of the softer recrystallized B-component for basal$\langle a\rangle$ slip. The conclusion is supported by the fact that the B-component is much more dominant in the recrystallized than in the host *c*-axis fabric. The dominance of the B-component with increasing recrystallization could explain why *c*-axis fabrics are apparently rotated *with* the sense of shear found in many naturally sheared quartzites.

(4) A deformation-based model of dynamic recrystallization also predicts that favorably oriented grains for easy slip systems grow at the expense of unfavorably oriented grains. Newly nucleated soft B-grains grow at the expense of hard A-, C- and D-grains and dominate the texture.

Acknowledgements

We wish to thank Richard Law and Jan Tullis for constructive reviews of the manuscript. HRW is grateful for awards from JSPS that made the collaboration with Japanese scientists possible. His research was also supported by NSF EAR-94-17580 and IGPP-LANL. RL acknowledges a Fulbright Fellowship to visit Berkeley.

References

Ave Lallement, H.G., Carter, N.L., 1971. Pressure dependence of quartz deformation lamellae orientations. Am. J. Sci. 270, 218–235.

Berthé, D., Choukroune, P., Jegouzo, P., 1979. Orthogneiss, mylonite and non-coaxial deformation of granites: the example of the South Armoricain shear zone. J. Struct. Geol. 1, 31–42.

Bouchez, J.L., 1977. Plastic deformation of quartzite at low temperature in area of natural strain gradient. Tectonophysics 39, 25–50.

Brunel, M., 1980. Quartz fabrics in shear-zone mylonites: evidence for a major imprint due to late strain increments. Tectonophysics 64, 33–44.

Canova, G.R., Wenk, H.-R., Molinari, A., 1992. Deformation modeling of multiphase polycrystals: case of a quartz–mica aggregate. Acta Metall. Mater. 40, 1519–1530.

Dawson, P., Beaudoin, R., 1998. Finite element modeling of heterogeneous plasticity. In: Kocks, U.F., Tomé, C., Wenk, H.-R. (Eds.), Texture and Anisotropy. Preferred Orientations in Polycrystals and Their Effect on Materials Properties. Cambridge University Press, Cambridge, pp. 512–531.

Dell' Angelo, L.N., Tullis, J., 1989. Fabric development in experimentally sheared quartzites. Tectonophysics 169, 1–21.

Fliervoet, T.F., White, S.H., 1995. Quartz deformation in a very fine grained quartzo-feldspathic mylonite: a lack of evidence for dominant grain boundary sliding deformation. J. Struct. Geol. 17, 1095–1109.

Flinn, D., 1962. On folding during three dimensional progressive deformation. J. Geol. Soc. London 118, 385–433.

Gleason, G.C., Tullis, J., Heidelbach, F., 1993. The role of dynamic recrystallization in the development of lattice preferred orientations in experimentally deformed quartz aggregates. J. Struct. Geol. 15, 1145–1168.

Gottstein, G., Mecking, H., 1985. Recrystallization. In: Wenk, H.-R. (Ed.), Preferred Orientation in Deformed Metals and Rocks: An Introduction to Modern Texture Analysis. Academic Press, Orlando, pp. 183–218.

Helming, K., Wenk, H.-R., Choi, C.S., Schafer, W., 1994. Description of quartz texture components: examples from metamorphic rocks. In: Bunge, H.-J., Siegesmund, S., Skrotzki, W., Weber, K. (Eds.), Textures in Geological Materials. Dtsch. Ges. Metallkunde, Oberursel, pp. 303–325.

Herwegh, M., Handy, M.R., 1996. The evolution of high-temperature mylonitic microfabrics: evidence from simple shearing of a quartz analogue (norcamphor). J. Struct. Geol. 18, 689–710.

Hirth, G., Tullis, J., 1992. Dislocation creep regimes in quartz aggregates. J. Struct. Geol. 14, 145–159.

Hobbs, B.E., 1968. Recrystallization of single crystals of quartz. Tectonophysics 6, 353–401.

Humphreys, F.J., Hatherly, M., 1995. Recrystallization and Related Annealing Phenomena. Oxford Univ. Press, Oxford.

Jessell, M.W., 1988a. Simulation of fabric development in recrystallizing aggregates, I. Description of the model. J. Struct. Geol. 10, 771–778.

Jessell, M.W., 1988b. Simulation of fabric development in recrystallizing aggregates, II. Example model runs. J. Struct. Geol. 10, 779–793.

Kocks, U.F., Tomé, C., Wenk, H.-R., 1998. Texture and Anisotropy. Preferred Orientations in Polycrystals and Their Effect on Materials Properties. Cambridge University Press, Cambridge.

Kunze, K., Pieri, M., Burlini, L., Wenk, H.-R., 1998. Texture development in calcite during deformation and recrystallization. Interpretation of high strain torsion experiments. EOS, Trans. Am. Geophys. Union 79, suppl., F851.

Law, R.D., 1987. Heterogeneous deformation and quartz crystallographic fabric transitions: natural examples from the Moine Thrust zone at the stack of Glencoul, northern Assynt. J. Struct. Geol. 9, 819–833.

Law, R.D., 1990. Crystallographic fabrics: a selective review of their applications to research in structural geology. In: Knipe, R.J., Rutter, E.H. (Eds.), Deformation Mechanisms, Rheology and Tectonics. Geol. Soc. Spec. Publ. 54, 335–352.

Law, R.D., Knipe, R.J., Dayan, H., 1984. Strain path partitioning within thrust sheets: microstructural and petrofabric evidence from the Moine Thrust zone at Loch Eriboll, northwest Scotland. J. Struct. Geol. 6, 477–497.

Lebensohn, R., Tomé, C., 1993. A self-consistent approach for the simulation of plastic deformation and texture development of polycrystals: application to zirconium alloys. Acta Metall. Mater. 41, 2611–2624.

Lebensohn, R., Tomé, C., 1994. A self-consistent visco-plastic model: calculation of rolling textures of anisotropic materials. Mater. Sci. Eng. A 175, 71–82.

Lebensohn, R., Gonzalez, M.I., Pochettino, A., Tomé, C., 1996. Measurement and prediction of texture development during a rolling sequence of zircaloy-4 tubes. J. Nuclear Mater. 229, 57–64.

Lebensohn, R., Wenk, H.-R., Tomé, C., 1998. Modelling deformation and recrystallization textures in calcite. Acta Metall. Mater. 46, 2683–2693.

Lister, G.S., 1977. Discussion. Cross-girdle *c*-axis fabrics in quartzites plastically deformed by plane strain and progressive simple shear. Tectonophysics 39, 51–54.

Lister, G.S., Dornsiepen, U.F., 1982. Fabric transition in the Saxony granulite terrain. J. Struct. Geol. 4, 81–92.

Lister, G.S., Hobbs, B.E., 1980. The simulation of fabric development during plastic deformation and its application to

quartzite: the influence of deformation history. J. Struct. Geol. 2, 355–370.

Lister, G.S., Williams, P.F., 1979. Fabric development in shear zones: theoretical controls and observed phenomena. J. Struct. Geol. 1, 283–297.

Lloyd, G.E., Freeman, B., 1991. SEM electron channeling analysis of dynamic recrystallization in a quartz grain. J. Struct. Geol. 13, 945–953.

Lloyd, G.E., Freeman, B., 1994. Dynamic recrystallization of quartz under greenschist conditions. J. Struct. Geol. 16, 867–881.

McLaren, A.C., 1986. Some speculations on the nature of high-angle grain boundaries in quartz rocks. In: Hobbs, B.E., Heard, H.C. (Eds.), Mineral and Rock Deformation: Laboratory Studies. Am. Geophys. Union, Geophys. Monogr. 36, 233–245.

Molinari, A., Canova, G., Ahzi, S., 1987. A selfconsistent approach of the large deformation polycrystal viscoplasticity. Acta Metall. 35, 2983–2994.

Platt, J.P., Vissers, R.L.M., 1980. Extensional structures in anisotropic rocks. J. Struct. Geol. 2, 397–410.

Schmid, S.M., Casey, M., Starkey, J., 1981. An illustration of the advantages of a complete texture analysis described by the orientation distribution function (ODF) using quartz pole figure data. Tectonophysics 78, 101–117.

Tagami, M., Takeshita, T., 1996. Deformation microstructures of the quartz in quartz schist from the Sambagawa metamorphic belt in central Shikoku. J. Geol. Soc. Jpn. 102, xi–xii.

Takeshita, T., 1996. Estimate of the physical conditions for deformation based on *c*-axis fabric transitions in naturally deformed quartzite (in Japanese with English abstract). J. Geol. Soc. Jpn. 102, 211–222.

Takeshita, T., Ise, K., 1994. Structural geology in the area along the Itoigawa–Shizuoka Tectonic Line in the east of Mt. Ho-oh, Yamanashi Prefecture, Part I (in Japanese with English abstract). Struct. Geol. (Kouzou Chishitsu) 40, 117–129.

Takeshita, T., Wenk, H.-R., 1988. Plastic anisotropy and geometrical hardening in quartzites. Tectonophysics 149, 345–361.

Taylor, G.I., 1938. Plastic strain in metals. J. Inst. Met. 62, 307–324.

Wenk, H.-R., 1973. The structures of the Bergell Alps. Eclogae Geol. Helv. 66, 255–291.

Wenk, H.-R., 1999. A voyage through the deformed Earth with the self-consistent model. Model. Mater. Sci. Eng. (in press)

Wenk, H.-R., Tomé, C., 1999. Recrystallization of olivine deformed in simple shear. J. Geophys. Res., in press.

Wenk, H.-R., Canova, G., Molinari, A., Kocks, U.F., 1989. Viscoplastic modeling of texture development in quartzite. J. Geophys. Res. 94, 17895–17906.

Wenk, H.-R., Canova, G., Bréchet, Y., Flandin, L., 1997. A deformation-based model for recrystallization of anisotropic materials. Acta Mater. 45, 3283–3296.

Wenk, H.-R., Matthies, S.S., Donovan, J., Chateigner, D.J., 1998. BEARTEX, a Windows-based program system for quantitative texture analysis. J. Appl. Crystallogr. 31, 262–269.

Zhang, S., Karato, S.-I., 1995. Lattice preferred orientation of olivine aggregates deformed in simple shear. Nature 375, 774–777.